SF 298 MASTER COPY KEEP THIS COPY FOR REPRODUCTION PURPOSES

REPORT DOCUMENTATION PAGE

Form Approved
OMB NO. 0704-0188

1. AGENCY USE ONLY (Leave blank)	2. REPORT DATE	3. REPORT TYPE AND DATES COVERED
	12/4/96	07/01/94-06/30/96 Final

4. TITLE AND SUBTITLE
Nonlinear Dynamics and Control of Wings and Panels

5. FUNDING NUMBERS
F49620-94-1-0382

6. AUTHOR(S)
Earl H. Dowell, P.I.
Lawrence Virgin, co-P.I.
Robert Clark, co-P.I.

7. PERFORMING ORGANIZATION NAMES(S) AND ADDRESS(ES)
Duke University
Office of Research Support
002, Allen Building
Durham, NC 27708-0077

AFOSR-TR-97
0159

9. SPONSORING / MONITORING AGENCY NAME(S) AND ADDRESS(ES)
AFOSR/NA
110 Duncan Avenue Suite B115
Bolling AFB DC 20332-0001

NA

10. SPONSORING / MONITORING AGENCY REPORT NUMBER
94-1-0382

11. SUPPLEMENTARY NOTES
The views, opinions and/or findings contained in this report are those of the author(s) and should not be construed as an official Department of the Air Force position, policy or decision, unless so designated by other documentation.

12a. DISTRIBUTION / AVAILABILITY STATEMENT
Approved for public release; distribution unlimited.

12b. DISTRIBUTION CODE

19970602 128

13. ABSTRACT *(Maximum 200 words)*

A multidisciplinary team of experts in aeroelasticity, control and nonlinear dynamics will study experimentally and theoretically the control of prototypical aeroelastic systems. Emphasis will be given to those systems with significant nonlinear characteristics, e.g. freeplay structural behavior and aeroelastic stall behavior for airfoils and wings and geometrical structural behavior and aeroelastic stall behavior for airfoils and wings and geometric structural nonlinearities of panels (plates and shells). Research in nonlinear dynamics has reached a level of relative maturity such that applications to real engineering systems (including physical experiments) are the next major advance. Adaptive control strategies will be employed to attenuate both persistent and impulsive disturbances for

14. SUBJECT TERMS	15. NUMBER IF PAGES 16
	16. PRICE CODE

17. SECURITY CLASSIFICATION OF REPORT	18. SECURITY CLASSIFICATION OF THIS PAGE	19. SECURITY CLASSIFICATION OF ABSTRACT	20. LIMITATION OF ABSTRACT
UNCLASSIFIED	UNCLASSIFIED	UNCLASSIFIED	UL

NSN 7540-01-280-5500

Enclosure 1

Standard Form 298 (Rev. 2-89)
Prescribed by ANSI Std. 239-18
298-102

REPORT DOCUMENTATION PAGE (SF298)
(Continuation Sheet)

nonlinear mechanical and aeroelastic systems will be used to aid in the design of distributed control structures with a focus on model-intensive control algorithms.

Enclosure 2

2. Objectives

The objectives are to create and evaluate theoretical and experimental methods for active control of nonlinear aeroelastic systems.

3. Status of effort

Considerable progress has been made toward achieving the research objectives. Both mathematical and experimental models have been completed, and excellent agreement has been achieved between results from the two complementary approaches. The uncontrolled model has been fully evaluated and initial results obtained for the model with active control as well. This project is right on schedule.

4. Accomplishments/New Findings

The successful correlation between theory and experiment has resulted in the production of four journal papers (see below). As mentioned above, the models are now being used to develop and assess various control strategies which aim to increase the flutter speed of this aeroelastic system.

5. Personnel Supported

The grant provides partial support for the two co-PI's, and half-time support of the Research Associate Deman Tang. Also, the associated AASERT award provides support for Mark Conner, a graduate student in the department of Mechanical Engineering and Materials Science. Part of this research has formed the basis for his PhD dissertation which was completed this past summer.

6. Publications

The four publications which are in various stages of completion are:

1) M.D. Conner, L.N. Virgin and E.H. Dowell (1995) "A note on accurate numerical integration of state-space models for aeroelastic systems with freeplay". Accepted for publication in the AIAA journal.

2) M.D. Conner, D.M. Tang, E.H. Dowell and L.N. Virgin (1995) "Nonlinear behavior of a typical section with control surface freeplay: Theoretical and Experimental Study". Accepted for publication in the Journal of Fluids and Structures.

3) K.D. Frampton, R.L. Clark and E.H. Dowell (1996) "State-Space Modeling for Aeroelastic Panels with Linearized Potential Flow Aerodynamic Loading". Accepted for publication in the Journal of Aircraft, Vol. 33, No. 4, 1996, pp. 816-822.

4) K.D. Frampton, R.L. Clark and E.H. Dowell (1996) "Active Control of Panel Flutter with Piezoelectric Transducers". Accepted for publication in the Journal of Aircraft, Vol. 33, No 4, 1996, pp. 768-774.

7. Interactions/Transitions

A number of presentations and seminars have been given connected with the parent award. For the AASERT award, Mark Conner attended a conference to present these results, and PI's have also presented some of these research findings at various workshops and professional society meetings including the AFOSR Workshop in Virginia Beach this summer.

8. New discoveries, inventions, or patent disclosures

Initial indications are that the flutter speed of this type of airfoil can be significantly increased based on numerical simulations and experimental measurements. Some specialized techniques from nonlinear dynamics have been used for the first time on an aeroelastic system. No patents have been issued.

9. Honors/Awards

One of the PI's (E.H. Dowell) is a member of the National Academy of Engineering. L.N. Virgin recently received tenure and promotion to Associate Professor, and R.L. Clark was recently awarded a prestigious CAREER award from the National Science Foundation.

JOURNAL OF AIRCRAFT
Vol. 33, No. 4, July–August 1996

Active Control of Panel Flutter with Piezoelectric Transducers

Kenneth D. Frampton,* Robert L. Clark,† and Earl H. Dowell‡
Duke University, Durham, North Carolina 27708-0302

This article investigates the active control of panel flutter with piezoelectric transducers and including linearized potential flow aerodynamics. The aerodynamic modeling is accomplished by approximating the aerodynamic generalized forces with infinite impulse response filters. These filters are coupled to the in vacuo panel dynamic system in feedback, thus, creating a coupled, aeroelastic system. The panel model is developed from a Rayleigh–Ritz approach and includes the mass and stiffness effects of a piezoelectric transducer. Acting as a self-sensing actuator, the piezoelectric transducer is used to implement direct rate feedback control. Results of an analytical implementation of this control system demonstrate a significant increase in the flutter boundaries.

Nomenclature

A, B, F, G = state-space matrices
a = panel length, chord
a_∞ = speed of sound
b = panel width, span
C_p = piezoelectric capacitance matrix
D = $EI/(1-\nu^2)$, stiffness
D_{mn} = aerodynamic influence coefficient
d_{31} = piezoelectric constant
$H_{mn}(t)$ = aerodynamic influence function
h = thickness
$I_{mn}(t)$ = aerodynamic influence function
i = output current vector
K = stiffness matrix
M = Mach number
M_p = structural mass matrix
M_s = piezo mass matrix
N = number of expansion modes
$\hat{P}(z)$ = approximate z-transfer function
$p(x, y, t)$ = aerodynamic pressure
$Q_n(t)$ = generalized force
$q_n(t)$ = generalized coordinate
$r_n(s)$ = $q_n(s)/h_s$
S_{mn} = aerodynamic influence coefficient
S_p = piezo area moment of inertia
s = tU_a/a
t = time
U_a = freestream velocity
u = state-space input vector
$\hat{v}$ = $v_n/v_{\max}$
$v_{\max}$ = piezo saturation voltage
v_n = input voltage
$w(x, y, t)$ = panel displacement
x, y, z = Cartesian coordinates
x = state vector
y = output vector
α, γ = Fourier transform variables
ε = $d_{31}v_{\max}a^2E_pS_p/D_ph_s(1-\nu_p)$
Θ = electromechanical coupling matrix
λ = $\rho_aU_a^2a^3/D$
μ_a = ρ_aa/ρ_sh_s
μ_p = ρ_ph_p/ρ_sh_s
ρ = density
σ = D_p/D_s
τ = integration dummy variable
$\phi(x, y, z, t)$ = fluid velocity potential
$\Psi_n(x, y)$ = modal expansion functions

Subscripts
a = aerodynamic
m, n = modal indices
p = piezoelectric
s = structural

Received May 21, 1995; revision received Jan. 24, 1996; accepted for publication Feb. 12, 1996.

*Graduate Research Assistant, Department of Mechanical Engineering and Materials Science. Student Member AIAA.

†Assistant Professor, Department of Mechanical Engineering and Materials Science. Member AIAA.

‡J. A. Jones Professor and Dean, School of Engineering, Department of Mechanical Engineering and Materials Science. Fellow AIAA.

Introduction

THE recent emergence of technology capable of performing the necessary computational and actuation tasks has led to the application of active control to many problems in dynamics. However, while much attention has been focused in the literature on active control of wing flutter, very little has been done in the area of panel flutter control. The phenomena of panel flutter has been studied for many years, but the few available references that apply active control to panel flutter use piston theory or quasisteady aerodynamics as the working model.[1,2] The use of piston theory is not without good reason since it is reasonably accurate at higher Mach numbers and modeling the effects of linearized potential flow (which is necessary for Mach numbers below 1.5), in a state-space representation suitable for control investigations is difficult. However, it is the transonic and low supersonic range that is usually most critical for flutter. For this reason, the inclusion of full potential flow aerodynamics is important to effective control system design.

This article investigates the active control of panel flutter including linearized potential flow aerodynamics. Development of the aeroelectroelastic model consists of combining the electroelastic panel model developed by Hagood et al.[3] with the aeroelastic panel model introduced by Frampton et al.[4] The electroelastic panel model combines the dynamics of a plate with the dynamics of piezoelectric transducers through a Rayleigh–Ritz formulation. The aeroelastic panel model is created by coupling a set of aerodynamic force approximating filters in feedback with an in vacuo panel model. The set of filters is constructed from the aerodynamic influence functions as developed by Dowell,[5,6] using Prony's method.

The control scheme used in this investigation is direct rate feedback (DRFB). This is implemented by using a piezoelec-

tric transducer simultaneously as a sensor and actuator as described by Anderson et al.,[7] Dosch and Inman,[8] and more recently Cole and Clark.[9] The piezoelectric transducer sensor signal, which is proportional to the strain rate, is amplified and fed back to itself as a control signal.

The effectiveness of this control system in delaying the onset of flutter is presented. In addition, the importance of considering full potential flow aerodynamics in a control system design is demonstrated. Also, the effect of piezoelectric transducer saturation is addressed.

Aeroelectroelasticity

Panel and Piezoelectric Transducer Dynamics

The panel in this investigation combines the aeroelastic modeling introduced by Frampton et al.[4] with the electroelastic modeling described by Hagood et al.[3] This method employs a Rayleigh–Ritz formulation to discretize the coupled equations of motion for the piezoelectric sensor/actuator and the aeroelastic panel. The combination of the two, which includes the mass and stiffness effects of the panel and the piezoelectric transducer, is referred to as an aeroelastic piezostructure.

This method assumes a separable solution using the in vacuo panel eigenfunctions and generalized coordinates of the form

$$w(x, y, t) = \sum_{n=1}^{N} \Psi_n(x, y) q_n(t) \tag{1}$$

and a linear voltage distribution across the piezoelectric thickness. The resulting actuation equations of motion with no structural damping are

$$[M_s + M_p]\{\ddot{q}\} + [K_s + K_p]\{q\} = [\Theta]\{v\} - \rho_a U_a^2 \{Q\} \tag{2}$$

and the rate sensor equations are

$$[\Theta]^T\{\dot{q}\} + [C_p]\{\dot{v}\} = \{i\} \tag{3}$$

where

$$\{q\} = \{q_1 \quad q_2 \quad \cdots \quad q_n\}^T \tag{4}$$

$$\{Q\} = \{Q_1 \quad Q_2 \quad \cdots \quad Q_n\}^T \tag{5}$$

$$\{v\} = \{v_1 \quad v_2 \quad \cdots \quad v_n\}^T \tag{6}$$

The aerodynamic generalized forces Q_n are a function of the aerodynamic pressure

$$Q_n(t) = \int_0^b \int_0^a \frac{p(x, y, t)}{\rho_a U_a^2} \Psi_n(x, y)\, dx\, dy \tag{7}$$

Definitions of the previous matrices can be found in Ref. 3. The coordinate system for the panel is shown in Fig. 1.

Full Potential Flow Generalized Forces

Consider the case of a simply supported panel with the following eigenfunctions (only one mode in the y direction is used for simplicity):

$$\Psi_n(x, y) = \sin[(n\pi/a)x]\sin[(\pi/b)y] \tag{8}$$

In this case the panel equation of motion [Eq. (2)] can be expressed nondimensionally as

$$[\hat{M}_s + 4\mu_p \hat{M}_p]\{\ddot{r}\} + \left[\frac{\mu_a}{\lambda}\hat{K}_s + 4\frac{\mu_a \sigma}{\lambda}\hat{K}_p\right]\{r\} = 8\frac{\mu_a \sigma \varepsilon}{\lambda}[\hat{\Theta}]\{\hat{v}\} - 4\mu_a\{\hat{Q}\} \tag{9}$$

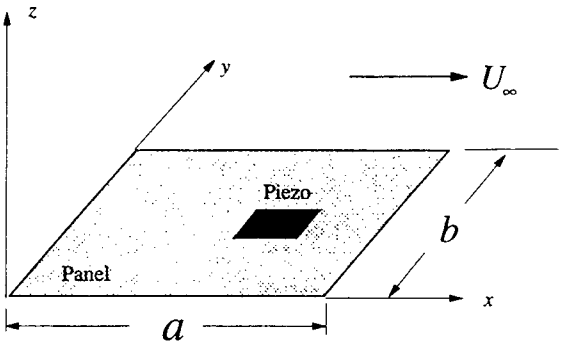

Fig. 1 Panel coordinate system.

where the hat [^], indicates that all dimensional terms have been pulled out of the matrix and included in the nondimensional coefficients.

The generalized forces $Q_n(t)$ are found by solving the partial differential equation describing the velocity potential in an inviscid, irrotational fluid moving parallel to the x axis

$$\nabla^2\phi - \frac{1}{a_\infty^2}\left[\frac{\partial^2\phi}{\partial t^2} + 2U_a\frac{\partial^2\phi}{\partial x \partial t} + U_a^2\frac{\partial^2\phi}{\partial x^2}\right] = 0 \tag{10}$$

subject to the boundary conditions for a panel embedded in an infinite baffle

$$\left.\frac{\partial\phi}{\partial z}\right|_{z=0} = \begin{cases} \dfrac{\partial w}{\partial t} + U_a\dfrac{\partial w}{\partial x} & \text{on the panel} \\ 0 & \text{off the panel} \end{cases} \tag{11}$$

and a finiteness or radiation condition as z approaches infinity.

The solution can be obtained by taking a Laplace transform with respect to time and a double Fourier transform with respect to the x and y spatial coordinates. The transformation is applied to Eqs. (10), (11), and Bernoulli's equation:

$$p = -\rho_a\left[\frac{\partial\phi}{\partial t} + U_a\frac{\partial\phi}{\partial x}\right] \tag{12}$$

while incorporating Eq. (1). Details of the solution process can be found in Refs. 5 and 6.

The solution yields the generalized aerodynamic forces on the panel that are given here as

$$Q_n(t) = \sum_{m=1}^{N} Q_{mn} \tag{13a}$$

where

$$Q_{mn}(t) = q_m(t)S_{mn} + \dot{q}_m(t)D_{mn} + \int_0^t q_m(\tau)H_{mn}(t - \tau)\, d\tau + \int_0^t \dot{q}_m(\tau)I_{mn}(t - \tau)\, d\tau \tag{13b}$$

$$S_{mn} = \frac{1}{M}\int_0^a \int_0^b \frac{\partial\Psi_m}{\partial x}\Psi_n\, dy\, dx \tag{13c}$$

$$D_{mn} = \frac{1}{MU_a}\int_0^a \int_0^b \Psi_m\Psi_n\, dy\, dx \tag{13d}$$

$$H_{mn}(t) = -\frac{U_a}{4\pi^2 M^2}\int_{-\infty}^{\infty}\int_{-\infty}^{\infty} G_{mn} i\alpha\sqrt{\alpha^2+\gamma^2}\,e^{-i\alpha U_a t} \times J_1[a_\infty t\sqrt{\alpha^2+\gamma^2}]\,d\alpha\,d\gamma \tag{13e}$$

$$I_{mn}(t) = -\frac{1}{4\pi^2 M^2}\int_{-\infty}^{\infty}\int_{-\infty}^{\infty} G_{mn}\sqrt{\alpha^2+\gamma^2}\,e^{-i\alpha U_a t} \times J_1[a_\infty t\sqrt{\alpha^2+\gamma^2}]\,d\alpha\,d\gamma \tag{13f}$$

$$G_{mn} = \int_0^a\int_0^b \Psi_m(x,y)e^{-i(\alpha x+\gamma y)}\,dy\,dx \times \int_0^a\int_0^b \Psi_n(x,y)e^{i(\alpha x+\gamma y)}\,dy\,dx \tag{13g}$$

The integrals in Eqs. (13c), (13d), and (13g) can be performed analytically for most panel eigenfunctions. Equations (13e) and (13f), which define the aerodynamic influence functions, must be evaluated numerically.

Piston Theory Generalized Forces

Piston theory is presented here for comparison with the full potential flow solution developed previously. Piston theory assumes that the pressure acting on the panel is equivalent to the pressure acting on a piston in a tube:

$$p = \rho_a a_\infty\left[\frac{\partial w}{\partial t} + U_a\frac{\partial w}{\partial x}\right] \tag{14}$$

The total piston velocity includes a convection term $U_a(\partial w/\partial x)$, as well as a direct velocity term $\partial w/\partial t$. Here the plate is the equivalent piston and the tube is perpendicular to the plate.

Combining Eqs. (1) and (14) and inserting into Eq. (7) yields the piston theory generalized aerodynamic forces

$$Q_n(t) = \sum_{m=1}^{N} Q_{mn} \tag{15a}$$

where

$$Q_{mn}(t) = q_m(t)S_{mn} + \dot{q}_m(t)D_{mn} \tag{15b}$$

$$S_{mn} = \frac{1}{M}\int_0^a\int_0^b \frac{\partial\Psi_m}{\partial x}\Psi_n\,dy\,dx \tag{15c}$$

$$D_{mn} = \frac{1}{MU_a}\int_0^a\int_0^b \Psi_m\Psi_n\,dy\,dx \tag{15d}$$

Note that this result is identical to that obtained from full potential flow analysis if the influence functions [$H_{mn}(t)$ and $I_{mn}(t)$] are ignored.

Approximate Generalized Forces

Since the generalized aerodynamic forces represented in Eq. (13b) are a function of the panel generalized coordinates, they can be viewed as dynamic feedback on the panel. These feedback dynamics are characterized by the influence functions $H_{mn}(t)$ and $I_{mn}(t)$, which represent aerodynamic impulse responses, and the influence coefficients S_{mn} and D_{mn}, which are instantaneous or feed-through dynamics.

Since there is no closed-form solution for the generalized forces some approximation must be made. The approach suggested here is to construct digital filters that approximate these dynamics. A reduced order recursive filter may be constructed by applying Prony's method to the aerodynamic influence functions.[10,11] Prony's method approximates an impulse response (in this case the influence functions) with a set of exponential functions in a least-squares sense. These exponential

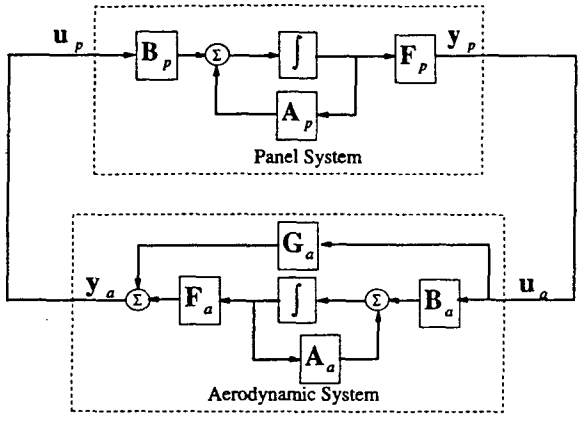

Fig. 2 State-space schematic of the complete aeroelastic system.

approximations to the influence functions can be readily transformed into an Ith order infinite impulse response (IIR) filter of the form

$$\hat{P}_{mn}(z) = \sum_{i=0}^{I-1} a_i z^{-i} \Big/ \sum_{i=0}^{I-1} b_i z^{-i} \tag{16}$$

As an example, suppose the values of the influence function $H_{mn}(iT)$ are used to solve for the filter coefficients in Eq. (16). When provided with an input signal that represents the panel generalized coordinate $q_m(iT)$, this filter would output an approximate convolution of $q_m(iT)$ with $H_{mn}(iT)$. Similarly, a filter could be constructed from $I_{mn}(iT)$ and provided with a signal representing $\dot{q}_m(iT)$. Summing the outputs of the two filters would yield an approximation to the dynamic portion of Eq. (13b). Details of this process may be found in Ref. 4.

An approximate filter can be found, as shown previously, for each aerodynamic influence function $H_{mn}(t)$ and $I_{mn}(t)$. A complete set of these filters can then be summed according to Eqs. (13a) and (13b). This would yield a dynamic system that has the generalized coordinates $q_m(t)$ and $\dot{q}_m(t)$ as the inputs and the generalized aerodynamic forces $Q_n(t)$ as the outputs. This system is then coupled as feedback on the panel resulting in a complete aeroelastic system. This is shown schematically (in state-space notation) in Fig. 2.

State-Space Formulation

The actuation equations of motion for the panel described in Eq. (2) can be expressed in state variable form as

$$\dot{x}_s = A_s x_s + B_s u_s \tag{17a}$$

$$y_s = F_s x_s \tag{17b}$$

where

$$x_s = \begin{Bmatrix} q \\ \dot{q} \end{Bmatrix}, \quad u_s = \begin{Bmatrix} Q(t) \\ v_p(t) \end{Bmatrix}, \quad y = \begin{Bmatrix} q \\ \dot{q} \\ i(t) \end{Bmatrix} \tag{17c}$$

$$A_s = \begin{bmatrix} 0 & I \\ -[M_s + M_p]^{-1}[K_s + K_p] & 0 \end{bmatrix} \tag{17d}$$

$$B_s = \begin{bmatrix} 0 & 0 \\ \rho_a U_a^2[M_s + M_p]^{-1} & [M_s + M_p]^{-1}\Theta \end{bmatrix} \tag{17e}$$

$$F_s = \begin{bmatrix} I \\ \Theta^T \end{bmatrix} \tag{17f}$$

The approximate filters of Eq. (16) can be converted to state-space form.[12] Each approximate filter associated with the influence function $H_{mn}(t)$ and $I_{mn}(t)$ has a state-space representation with matrices $\{A_{H_{mn}}, B_{H_{mn}}, F_{H_{mn}}, G_{H_{mn}}\}$ and $\{A_{I_{mn}}, A_{I_{mn}}, F_{I_{mn}}, G_{I_{mn}}\}$, respectively. The complete set of state-space repre-

sentations can be assembled to form the approximate aerodynamic system as follows:

$$\boldsymbol{x}_a = A_a \boldsymbol{x}_a + B_a \boldsymbol{u}_a \tag{18a}$$

$$\boldsymbol{y}_a = F_a \boldsymbol{x}_a + G_a \boldsymbol{u}_a \tag{18b}$$

where

$$\boldsymbol{y}_a = \{Q_1(t) \quad Q_2(t) \quad \cdots \quad Q_n(t)\}^T \tag{18c}$$

$$\boldsymbol{u}_a = \{q_1 \quad \dot{q}_1 \quad q_2 \quad \dot{q}_2 \quad \cdots \quad q_n \quad \dot{q}_n\}^T \tag{18d}$$

$$A_a = \begin{bmatrix} A_{H_{11}} & 0 & \cdots & 0 & 0 \\ 0 & A_{I_{11}} & \cdots & 0 & 0 \\ \vdots & \vdots & \ddots & \vdots & \vdots \\ 0 & 0 & \cdots & A_{H_{mn}} & 0 \\ 0 & 0 & \cdots & 0 & A_{I_{mn}} \end{bmatrix} \tag{18e}$$

$$B_a = \begin{bmatrix} B_{H_{11}} & 0 & \cdots & 0 & 0 \\ 0 & B_{I_{11}} & \cdots & 0 & 0 \\ \vdots & \vdots & \ddots & \vdots & \vdots \\ 0 & 0 & \cdots & B_{H_{1n}} & 0 \\ 0 & 0 & \cdots & 0 & B_{I_{1n}} \\ \vdots & \vdots & \vdots & \vdots & \vdots \\ B_{H_{m1}} & 0 & \cdots & 0 & 0 \\ 0 & B_{I_{m1}} & \cdots & 0 & 0 \\ \vdots & \vdots & \ddots & \vdots & \vdots \\ 0 & 0 & \cdots & B_{H_{mn}} & 0 \\ 0 & 0 & \cdots & 0 & B_{I_{mn}} \end{bmatrix} \tag{18f}$$

$$F_a = \begin{bmatrix} F_{H_{11}} & F_{I_{11}} & \cdots & F_{H_{1n}} & F_{I_{1n}} \\ F_{H_{21}} & F_{I_{21}} & \cdots & F_{H_{2n}} & F_{I_{2n}} \\ \vdots & \vdots & \ddots & \vdots & \vdots \\ F_{H_{m1}} & F_{I_{m1}} & \cdots & F_{H_{mn}} & F_{I_{mn}} \end{bmatrix} \tag{18g}$$

$$G_a = \begin{bmatrix} G'_{H_{11}} & G'_{I_{11}} & \cdots & G'_{H_{1n}} & G'_{I_{1n}} \\ G'_{H_{21}} & G'_{I_{21}} & \cdots & G'_{H_{2n}} & G'_{I_{2n}} \\ \vdots & \vdots & \ddots & \vdots & \vdots \\ G'_{H_{m1}} & G'_{I_{m1}} & \cdots & G'_{H_{mn}} & G'_{I_{mn}} \end{bmatrix} \tag{18h}$$

and the influence coefficients are incorporated as follows:

$$G'_{H_{mn}} = G_{H_{mn}} + S_{mn} \tag{18i}$$

$$G'_{I_{mn}} = G_{I_{mn}} + D_{mn} \tag{18j}$$

The aerodynamic states $\boldsymbol{x}_a$ are of mathematical construct and have no physical significance. The panel and aerodynamic state-space models can then be coupled together as shown in Fig. 2.

The accuracy of this model can be demonstrated by comparing the flutter boundaries with those reported in the literature.[5,6,13,14] The flutter boundaries are determined by increasing the nondimensional dynamic pressure λ while holding all other parameters fixed. Flutter occurs when one of the system eigenvalues moves into the right-half-plane.

A comparison of flutter dynamic pressure vs Mach number is shown in Fig. 3. Results are illustrated for a panel with mass ratios of $\mu_a = 0.1$ and $\mu_p = 0.5$, $\sigma = 1.2$, $\varepsilon = 130$, and dimension ratio $a/b = 1$, using a four-mode panel model. The figure shows the flutter boundaries for the plate with and without a piezoelectric transducer for both full potential flow and piston theory aerodynamics. Note that the presence of the piezoelectric transducer slightly increases the flutter boundary. This is because of the increased panel mass with the transducer. Also note that the two aerodynamic theories approach each other asymptotically as the Mach number increases. However, for Mach numbers below 1.5 the theory incorporating linearized potential flow aerodynamics predicts flutter boundaries well below that predicted by piston theory. These results are consistent with those obtained by Dowell.[5,6] A more detailed discussion of the model validity can be found in Ref. 4.

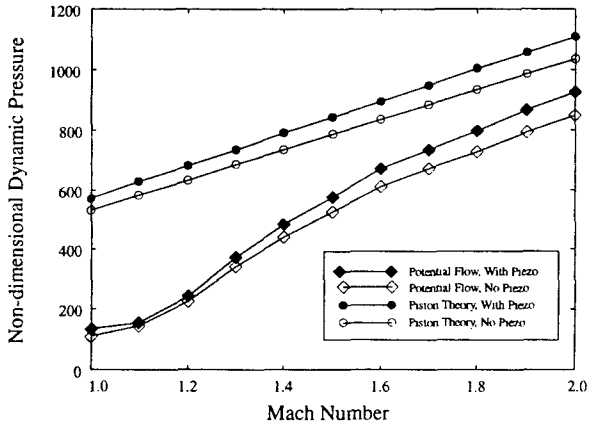

Fig. 3 λ_f vs M for a panel aspect ratio of $a/b = 1$.

Collocated Direct Rate Feedback Control

Collocated direct rate feedback control is a well-documented form of control which, in the absence of sensor/actuator dynamics and rigid body modes, has guaranteed stability for any positive feedback gain.[15]

Collocation is achieved by using a piezoceramic transduction device as a sensoriactuator,[9] i.e., simultaneously as a sensor and actuator.[7-9,16] By applying the appropriate circuitry to the piezoelectric transducer, the portion of the piezoelectric output that is proportional to the structural velocity can be isolated. This is equivalent to rendering Eq. (3) as

$$[\Theta]^T\{\dot{q}\} = \{i\} \tag{19}$$

Direct rate feedback control consists of feeding back a signal proportional to the sensor current i from Eq. (19) as the voltage input v to Eq. (2).

Results

The effectiveness of collocated direct rate feedback control is demonstrated by applying the control to the aeroelastic panel model and finding the flutter instability boundaries. All results in this section are for the following parameters: $\mu_p = 0.5$, $\mu_a = 0.1$, $\sigma = 1.2$, $\varepsilon = 130$, and $a/b = 1.0$. These parameters correspond to typical values for G-1195-type piezoceramic and a steel panel. Previous investigations have shown that mass ratio has relatively little effect on the flutter boundaries,[14] therefore, the mass ratios μ_p and μ_a are held constant.

Selection of the piezoelectric transducer location is very important for a successful control system design. Formal optimization of transducer location was not performed, however, investigation into the aeroelastic mode shapes suggests a good location. It is well known that piezoelectric transducers are most effective when located in regions of high strain (i.e., high panel curvature). Since the goal is to control flutter, the flutter mode shapes must be considered when looking for advantageous locations. This approach was also considered by Scott and Weisshaar.[1]

The normalized flutter mode shapes in the chordwise direction are shown in Fig. 4 for various Mach numbers. Note the strong influence of the 1st and 2nd in vacuo modes on the flutter mode. The region of maximum strain at each Mach number occurs very near $x/a = 0.7$. For this reason a transducer coverage of $0.6 < x/a < 0.8$ and $0.4 < y/b < 0.6$ was selected. This chordwise location also corresponds to the maximum delay in the migration of open loop zeros into the right-half-plane. The importance of the zero migration delay will be discussed in more detail later.

Results from this analysis are shown in Fig. 5 for the full potential flow model and several feedback gains. Figure 5 demonstrates that, except near $M = 1.0$, the use of direct rate feedback control is equally effective at all Mach numbers in terms of a percentage increase in flutter dynamic pressure. Note in Fig. 5 that there is a maximum flutter boundary that direct rate feedback can achieve. This is demonstrated by the coincidence of the flutter boundary for feedback gains of 0.1 and 0.2.

This behavior is better illustrated in Fig. 6, which shows the change in flutter nondimensional dynamic pressure with increasing feedback gain for three Mach numbers. Also included in Fig. 6 are similar results for a piston theory aerodynamic model. It is apparent in Fig. 6 that the piston theory model overpredicts the control effectiveness, particularly at lower Mach numbers, compared to the full potential flow model. Also note that the difference between the full potential flow model and the piston theory model increases with increasing gain.

An important result demonstrated in Fig. 6 is that, at a fixed Mach number, there is a maximum flutter dynamic pressure that direct rate feedback control can achieve. This is evident in the asymptotic behavior of the flutter boundaries with increasing gain shown in Fig. 6. In other words, for a fixed Mach number, there is a limiting nondimensional dynamic pressure λ, beyond which direct rate feedback control cannot stabilize the system.

This limitation is because of the mechanism by which direct rate feedback control stabilizes the system. Stabilization is accomplished by moving the open-loop poles toward the open-loop zeros. This is demonstrated in Fig. 7, which shows the closed-loop root locus for a four-mode panel (aerodynamic poles are omitted for clarity). Results in Fig. 7 are for a Mach number of 2.0 and dynamic pressure $\lambda = 1300$, which is greater than the open-loop flutter dynamic pressure, but less than the limiting dynamic pressure. Note in Fig. 7 that as the feedback gain is increased the unstable poles are drawn toward the open-loop zeros that are located in the left-half-plane. Therefore, given enough feedback gain, the system can be stabilized.

Unfortunately, it is not always the case that the open-loop zeros, toward which the unstable poles are drawn, lie in the left-half-plane. The location of these open-loop zeros is a function of M, mass ratio μ_a, the sensoriactuator location, and most strongly a function of the dynamic pressure λ. This dependence is demonstrated in Fig. 8, which shows the locus of the system zeros as a function of λ. This plot is for a Mach number of 2.0. Note the migration path of the zeros. At a dynamic pressure of $\lambda = 1593$, a pair of zeros moves into the right-half-plane. Piston theory predicts that the zero will move into the right-half-plane at a dynamic pressure of $\lambda = 1903$. This accounts for the large difference in maximum flutter dynamic pressure depicted in Fig. 6.

A root locus similar to that in Fig. 7, but with $\lambda = 1630$, is shown in Fig. 9. Note how the pair of unstable poles is moved toward a pair of zeros in the right-half-plane. Therefore, no amount of feedback gain could stabilize the system. The point at which the open-loop zeros moves into the right-half-plane is the closed-loop flutter boundary. Beyond this point, even with direct rate feedback control, the panel will flutter.

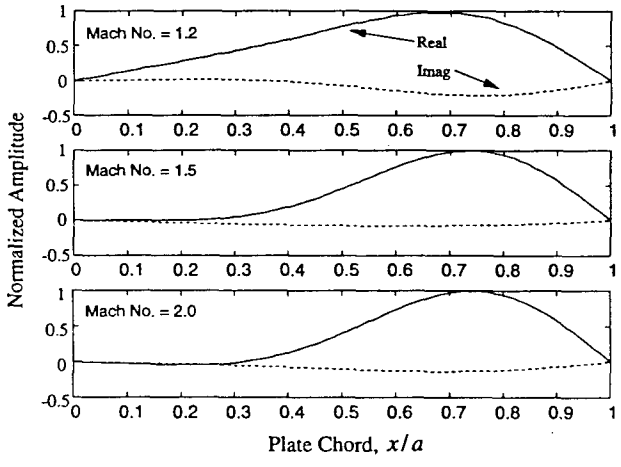

Fig. 4 Flutter mode shapes for various Mach numbers.

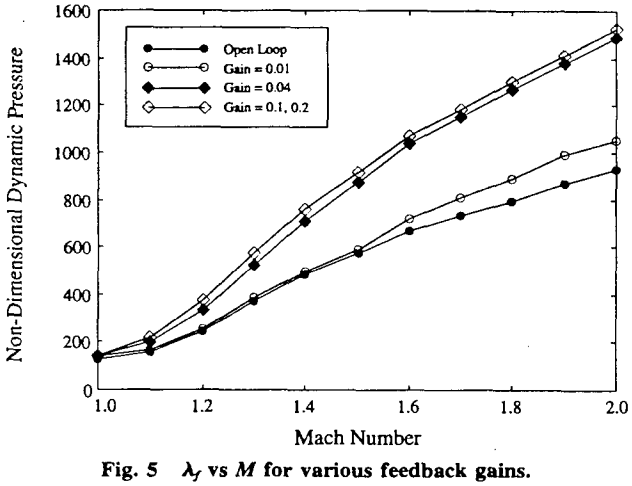

Fig. 5 λ_f vs M for various feedback gains.

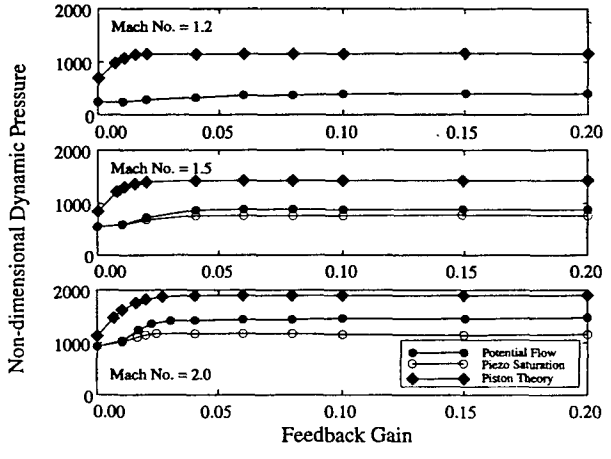

Fig. 6 Flutter boundaries with varying feedback gain.

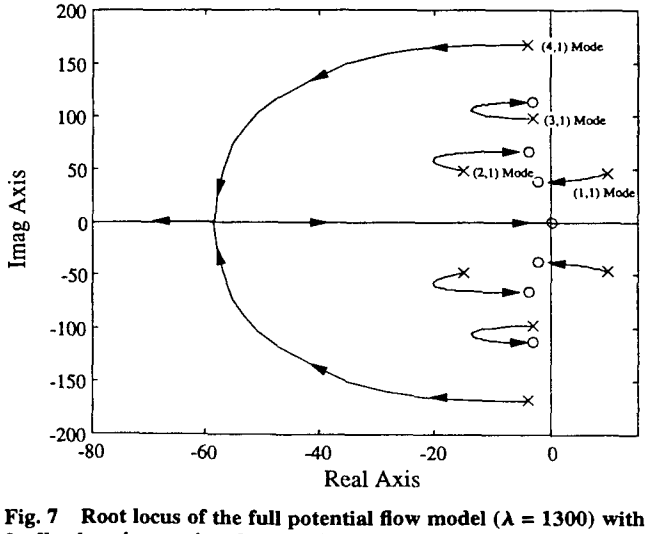

Fig. 7 Root locus of the full potential flow model ($\lambda = 1300$) with feedback gain varying from 0 (corresponding to the open-loop pole, x) to ∞ (corresponding to the open-loop zero, ○).

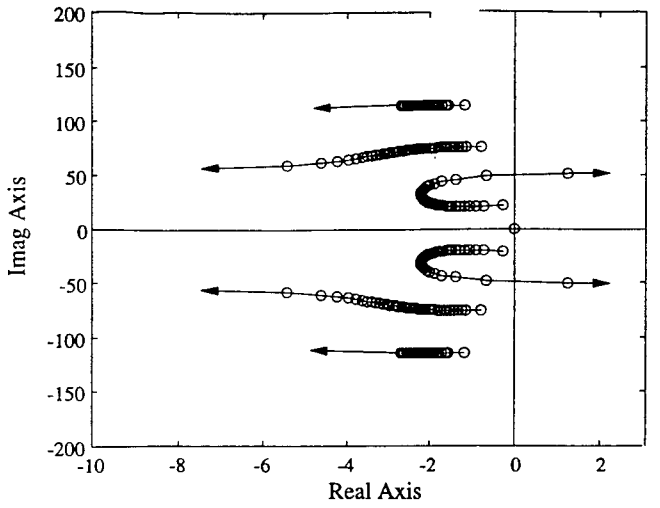

Fig. 8 Zero locus of the full potential flow model with nondimensional dynamic pressure varying from $\lambda = 0$ to $\lambda = 1600$ (○ = zero).

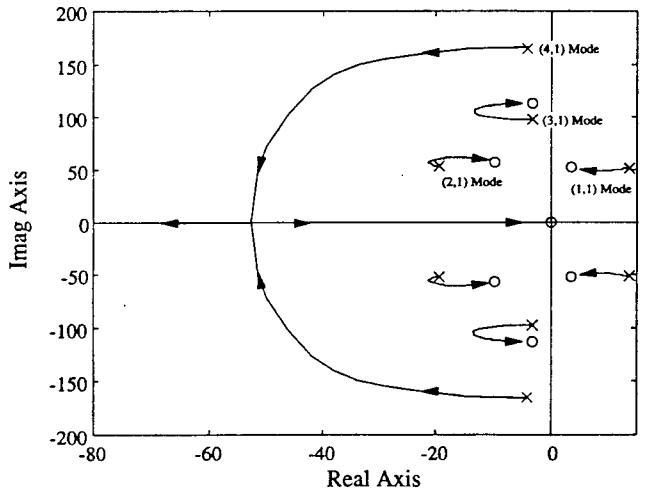

Fig. 9 Root locus of the full potential flow model ($\lambda = 1630$) with feedback gain varying from 0 (corresponding to the open-loop pole, ×) to ∞ (corresponding to the open-loop zero, ○).

Although this demonstrates a limit to the amount that direct rate feedback control can increase the flutter boundary, other feedback control techniques could potentially increase the boundary further. Since the migration of the open-loop zeros is, in part, a function of the location of the sensoriactuator, its size and location on the aeroelastic panel could be formally optimized to further delay the zero migration into the right-half-plane.

A second limitation in the effectiveness of DRFB flutter control is the saturation of the piezoelectric transducer. The applied control signal voltage is proportional to the strain rate and is therefore a function of the panel disturbance. In a realistic situation the disturbance would result from externally applied pressures such as turbulent boundary-layer (TBL) pressures. For simplicity in this investigation an initial displacement in the first mode of $r_1 = q_1/h_s = 1.0$ was used as the disturbance. The time history of the control signal was calculated for various Mach numbers and the dynamic pressure at which the maximum allowable piezoelectric voltage was reached was noted.

Results for transducer saturation are shown in Fig. 6. Note that for $M = 1.2$ the saturation curve corresponds with the potential flow flutter curve. Not until higher Mach numbers does the piezoelectric saturation significantly limit the ability to delay flutter onset. Considering piezoelectric saturation effects the flutter dynamic pressure is increased by 55% at $M = 1.2$, 28% at $M = 1.5$, and 26% at $M = 2.0$, as shown in Fig. 6.

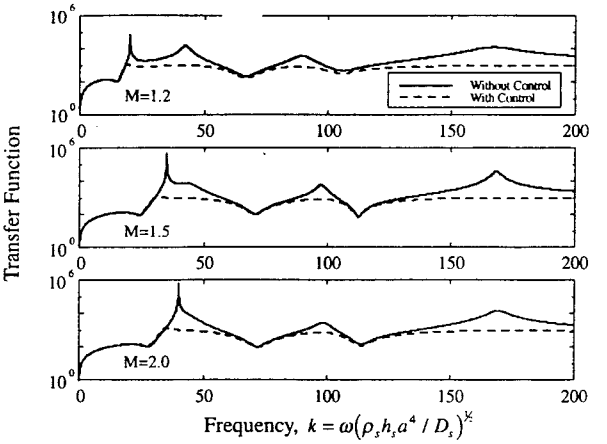

Fig. 10 Open- and closed-loop transfer functions.

Also note that while the application of collocated direct rate feedback control is effective for panel flutter control it is also effective for disturbance rejection. This is demonstrated in Fig. 10, which shows the open- and closed-loop transfer functions for three Mach numbers. In each case the dynamic pressure is just below the corresponding flutter dynamic pressure for that Mach number. The effect of direct rate feedback control in this case is to add damping to the near flutter poles, thus reducing the spectral peak.

Conclusions

The active control of panel flutter has been investigated including full linearized potential flow aerodynamic theory appropriate for the full transonic and supersonic Mach number range. Direct rate feedback control from a sensoriactuator piezoelectric transducer was modeled and its effectiveness in controlling flutter instability was demonstrated. It was shown that this type of control is capable of significantly increasing the flutter nondimensional dynamic pressure. It was also shown that this type of control is limited by the migration of the open-loop zeros into the right half-plane, thus, beyond a certain dynamic pressure, preventing the system from being stabilized. This zero migration to the right half-plane defines a new flutter boundary for the closed-loop aeroelastic panel. A second limitation was demonstrated in the saturation of the piezoelectric transducer.

Acknowledgments

This work was supported in part by the U.S. Air Force Office of Scientific Research, with Contract Monitor Jim Chang C.I.P.I., and the National Science Foundation Graduate Traineeship EE-92-56573.

References

[1]Scott, R. C., "Panel Flutter Suppression Using Adaptive Material Actuators," *Journal of Aircraft*, Vol. 31, No. 1, 1994, pp. 213–222.

[2]Hajela, P., "Application of Piezoelectric Elements in Supersonic Panel Flutter Suppression," AIAA Paper 91-3191, Sept. 1991.

[3]Hagood, N. W., Chung, W. H., and Von Flotow, A., "Modelling of Piezoelectric Actuator Dynamics for Active Structural Control," *Journal of Intelligent Material Systems and Structures*, Vol. 1, No. 3, 1990, pp. 327–354.

[4]Frampton, K. D., Clark, R. L., and Dowell, E. H., "State Space Modeling for Aeroelastic Panels Subject to Full Potential Flow Aerodynamic Loading," *Proceedings of the AIAA 36th Structures, Structural Dynamics, and Materials Conference* (New Orleans, LA), AIAA, Washington, DC, 1995, pp. 1183–1189.

[5]Dowell, E. H., "Generalized Aerodynamic Forces on a Flexible Plate Undergoing Transient Motion," *Quarterly of Applied Mathe-*

matics, Vol. 26, No. 3, 1967, pp. 2267–2270.

[6]Dowell, E. H., *Aeroelasticity of Plates and Shell*, Noordhoff International, Leyden, The Netherlands, 1975.

[7]Anderson, E. H., Hagood, N. W., and Goodliffe, J. M., "Self-Sensing Piezoelectric Actuation: Analysis and Application to Controlled Structures," *Proceedings of the AIAA 33rd Structures, Structural Dynamics, and Materials Conference* (Dallas, TX), AIAA, Washington, DC, 1992, pp. 2141–2155.

[8]Dosch, J. J., Inman, D. J., and Garcia, E., "A Self-Sensing Piezoelectric Actuator for Collocated Control," *Journal of Intelligent Material Systems and Structures*, Vol. 3, No. 1, 1992, pp. 166–185.

[9]Cole, D. G., and Clark, R. L., "Adaptive Compensation of Piezoelectric Sensoriactuators," *Journal of Intelligent Material Systems and Structures*, Vol. 5, No. 1, 1994, pp. 665–672.

[10]Evans, A. G., and Fischl, R., "Optimal Least Squares Time-Domain Synthesis of Recursive Digital Filters," *IEEE Transactions on Audio and Electroacoustics*, Vol. AU-21, No. 1, 1973, pp. 61–65.

[11]Marple, S. L., Jr., *Digital Spectral Analysis with Applications*, Prentice–Hall, Englewood Cliffs, NJ, 1987.

[12]Haykin, S., *Adaptive Filter Theory*, 2nd ed., Prentice–Hall, Englewood Cliffs, NJ, 1991.

[13]Hedgepeth, J. M., "Flutter of Rectangular Simply Supported Panels at High Supersonic Speeds," *Journal of the Aeronautical Sciences*, Vol. 24, No. 8, 1957, pp. 563–573.

[14]Johns, D. J., "A Panel Flutter Review," *Manual on Aeroelasticity*, Pt. III, AGARD, 1969, Chap. 7.

[15]Balas, M. J., "Direct Velocity Feedback Control of Large Space Structures," *Journal of Guidance, Control, and Dynamics*, Vol. 2, No. 3, 1979, pp. 252, 253.

[16]Vipperman, J. S., and Clark, R. L., "Hybrid Analog and Digital Adaptive Compensation of Piezoelectric Sensoriactuators," *Proceedings of the AIAA 36th Structures, Structural Dynamics, and Materials Conference* (New Orleans, LA), AIAA, Washington, DC, 1995, pp. 2854–2859.

JOURNAL OF AIRCRAFT
Vol. 33, No. 4, July–August 1996

State-Space Modeling for Aeroelastic Panels with Linearized Potential Flow Aerodynamic Loading

Kenneth D. Frampton,* Robert L. Clark,† and Earl H. Dowell‡
Duke University, Durham, North Carolina 27708

This article presents a new method for the state-space modeling of aeroelastic panels subject to linearized potential flow aerodynamic loading. This is accomplished by approximating the aerodynamic generalized forces on the panel with discrete, infinite impulse response (IIR) filters. The IIR filters are created using Prony's method for a least-squares-fit to the aerodynamic influence functions. These filters are coupled to the in vacuo panel dynamic system as feedback, creating a coupled, aeroelastic system. The accuracy of the model is established by comparing the panel flutter boundaries of the approximate system with those found in past studies.

Nomenclature

A, B, F, G	= state-space matrices
a	= panel length, chord
$a_i, \hat{a}_i$	= filter coefficients
a_∞	= speed of sound
b	= panel width, span
$b_i, \hat{b}_i$	= filter coefficients
D	= $EI/(1-\nu^2)$, panel stiffness
D_{mn}	= aerodynamic influence coefficient
$H_{mn}(t)$	= aerodynamic influence function
h	= panel thickness
I	= approximate infinite impulse response filter order
$I_{mn}(t)$	= aerodynamic influence function
$J_1[\cdot]$	= Bessel's function
M	= Mach number
M_n	= modal mass
N	= number of expansion modes
$P(z)$	= exact z transfer function
$\hat{P}(z)$	= approximate z transfer
$\hat{P}(\kappa)$	= approximate Laplace transfer function
$p(x, y, t)$	= aerodynamic pressure
$Q_n(t)$	= generalized force
$q_n(t)$	= generalized coordinate
R	= finite impulse response filter order
$r_n(s)$	= $q_n(t)/h$
S_{mn}	= aerodynamic influence coefficient
s	= tU_∞/a
T	= sample period
t	= time
U_a	= freestream velocity
u	= state-space input vector
$w(x, y, t)$	= panel displacement
x, y, z	= Cartesian coordinates
x	= state vector
y	= output vector
α, γ	= Fourier transform variables
κ	= Laplace domain variable
λ	= $\rho U_a^2 a^3/D$
μ	= $\rho_a a/\rho_p$
ρ_a	= density of fluid
ρ_p	= panel mass per area
τ	= integration dummy variable
$\phi(x, y, z, t)$	= fluid velocity potential
$\Psi_n(x, y)$	= modal expansion functions
ω_n	= modal natural frequency

Subscripts

a	= aerodynamic
m, n	= modal indices
p	= panel

Received May 21, 1995; revision received Dec. 2, 1995; accepted for publication Dec. 29, 1995.

*Graduate Research Assistant, Department of Mechanical Engineering and Materials Science. Student Member AIAA.

†Assistant Professor, Department of Mechanical Engineering and Materials Science. Member AIAA.

‡J. A. Jones Professor and Dean, School of Engineering. Fellow AIAA.

Introduction

PANEL flutter is the self-excited dynamic instability of plate-like structures exposed to fluid flow. This aeroelastic phenomenon has received much attention in the past and is very important toward the successful development of supersonic aircraft such as the National Aerospace Plane, the High Speed Civil Transport, and the Advanced Tactical fighter, to name a few. Dugundji[1] published an excellent paper on early investigations into linear panel flutter, whereas Gray and Mei[2] gave a review of more recent efforts including nonlinear effects. However, the vast majority of work has been performed assuming piston theory as the aerodynamic model. The use of piston theory is not without good reason, since it is reasonably accurate at higher Mach numbers and modeling the effects of linearized potential flow, which is necessary for lower Mach numbers ($M < 1.5$), is challenging. Since low supersonic flight speeds are utilized by many aircraft, it is important to consider the effects of full potential flow aerodynamic loading in panel flutter investigations.

The few references that include linearized potential flow aerodynamics focus on the determination of flutter boundaries, and subsequently, the limit cycle oscillations in the postflutter (nonlinear) regime. These models, however, are not conducive to the application of modern control theory. A method of building a state-space model of the coupled aeroelastic system would permit the determination of flutter boundaries as well as provide a means of applying modern control theory to the problem. While this has already been accomplished for typical wing sections,[3,4] it has yet to be done for panels.

This article presents a method for constructing a state-space model of the coupled aeroelastic panel including linearized potential flow aerodynamics. This is accomplished by approximating the aerodynamic generalized forces on a panel, as developed by Dowell,[5,6] with discrete, infinite impulse response

(IIR) filters. These filters are coupled to the in vacuo panel dynamic system as feedback, creating a coupled, aeroelastic system. The accuracy of the model is established by comparing the panel flutter boundaries of the approximate system with those found in the literature.[6-9]

Panel Dynamics and Generalized Forces

The partial differential equation (PDE) of motion describing a thin, uniform panel is[10]

$$D\left[\frac{\partial^4 w(x, y, t)}{\partial x^4} + \frac{\partial^4 w(x, y, t)}{\partial x^2 \partial y^2} + \frac{\partial^4 w(x, y, t)}{\partial y^4}\right] + \rho_p \frac{\partial^2 w(x, y, t)}{\partial t^2} + p(x, y, t) = 0 \quad (1)$$

The coordinate system for the panel is shown in Fig. 1.

A separable expansion solution is assumed using the in vacuo orthogonal panel eigenfunctions and generalized coordinates:

$$w(x, y, t) = \sum_{n=1}^{N} \Psi_n(x, y) q_n(t) \quad (2)$$

Substituting Eq. (2) into Eq. (1), multiplying by an arbitrary expansion function $\Psi_m(x, y)$, and integrating over the domain yields a set of ordinary differential equations of the form:

$$M_n[\ddot{q}_n(t) + \omega_n^2 q_n(t)] + \rho_a U_a^2 Q_n(t) = 0 \quad (3)$$

where

$$M_n = \int_0^b \int_0^a \rho_p \Psi_n \Psi_m \, dx \, dy \quad (4)$$

$$M_n \omega_n^2 = \int_0^b \int_0^a D\left[\frac{\partial^2 \Psi_n}{\partial x^2}\frac{\partial^2 \Psi_m}{\partial x^2} + \nu\left(\frac{\partial^2 \Psi_n}{\partial x^2}\frac{\partial^2 \Psi_m}{\partial y^2} + \frac{\partial^2 \Psi_m}{\partial x^2}\frac{\partial^2 \Psi_n}{\partial y^2}\right) + 2(1 - \nu^2)\frac{\partial^2 \Psi_n}{\partial x \partial y}\frac{\partial^2 \Psi_m}{\partial x \partial y} + \frac{\partial^2 \Psi_n}{\partial y^2}\frac{\partial^2 \Psi_m}{\partial y^2}\right] dx \, dy \quad (5)$$

and the generalized forces are a function of the aerodynamic pressure

$$Q_n(t) = \int_0^b \int_0^a \frac{p(x, y, t)}{\rho_a U_a^2} \Psi_n(x, y) \, dx \, dy \quad (6)$$

Full Potential Flow Generalized Forces

Consider the case of a simply supported panel with the following eigenfunctions (only one mode in the y direction for simplicity such that $n = 1, 2, \ldots, N$):

$$\Psi_n(x, y) = \sin[(n\pi/a)x]\sin[(\pi/b)y] \quad (7)$$

In this case, the panel equation of motion, Eq. (3), can be expressed nondimensionally as

$$\ddot{r}_n(s) + (\mu/\lambda)\pi^4[n^2 + (a/b)^2]^2 r_n(s) + 4\mu Q_n(s) = 0 \quad (8)$$

The generalized forces $Q_n(t)$ are found by solving the PDE describing the velocity potential in an inviscid, irrotational fluid moving parallel to the x axis

$$\nabla^2 \phi - \frac{1}{a_\infty^2}\left(\frac{\partial^2 \phi}{\partial t^2} + 2U_a \frac{\partial^2 \phi}{\partial x \partial t} + U_a^2 \frac{\partial^2 \phi}{\partial x^2}\right) = 0 \quad (9)$$

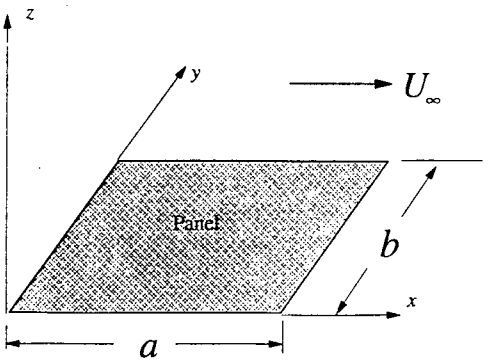

Fig. 1 Panel coordinate system.

subject to the boundary conditions for a panel embedded in an infinite baffle

$$\left.\frac{\partial \phi}{\partial z}\right|_{z=0} = \begin{cases} \dfrac{\partial w}{\partial t} + U_a \dfrac{\partial w}{\partial x} & \text{on the panel} \\ 0 & \text{off the panel} \end{cases} \quad (10)$$

and a finiteness or radiation condition as z approaches infinity.

The solution can be obtained by taking a Laplace transform with respect to time and a double Fourier transform with respect to the x and y spatial coordinates. The transformation is applied to Eqs. (9) and (10) and Bernoulli's equation,

$$p = -\rho_a\left(\frac{\partial \phi}{\partial t} + U_a \frac{\partial \phi}{\partial x}\right) \quad (11)$$

while incorporating Eq. (2). Details of the solution are discussed by Dowell.[5,6]

The solution yields the generalized aerodynamic forces on the panel, which are given here as

$$Q_n(t) = \sum_{m=1}^{N} Q_{mn}(t) \quad (12a)$$

where $Q_{mn}(t)$ is the force on the nth panel mode because of the motion of the mth panel mode, such that

$$Q_{mn}(t) = q_m(t)S_{mn} + \dot{q}_m(t)D_{mn} + \int_0^t q_m(\tau)H_{mn}(t - \tau) \, d\tau + \int_0^t \dot{q}_m(\tau)I_{mn}(t - \tau) \, d\tau \quad (12b)$$

$$S_{mn} = \frac{1}{M}\int_0^a \int_0^b \frac{\partial \Psi_m}{\partial x}\Psi_n \, dy \, dx \quad (12c)$$

$$D_{mn} = \frac{1}{MU_a}\int_0^a \int_0^b \Psi_m \Psi_n \, dy \, dx \quad (12d)$$

$$H_{mn}(t) = -\frac{U_a}{4\pi^2 M^2}\int_{-\infty}^{\infty}\int_{-\infty}^{\infty} G_{mn} i\alpha\sqrt{\alpha^2 + \gamma^2} e^{-i\alpha U_a t} \times J_1(a_\infty t\sqrt{\alpha^2 + \gamma^2}) \, d\alpha \, d\gamma \quad (12e)$$

$$I_{mn}(t) = -\frac{1}{4\pi^2 M^2}\int_{-\infty}^{\infty}\int_{-\infty}^{\infty} G_{mn}\sqrt{\alpha^2 + \gamma^2} e^{-i\alpha U_a t} \times J_1(a_\infty t\sqrt{\alpha^2 + \gamma^2}) \, d\alpha \, d\gamma \quad (12f)$$

$$G_{mn} = \int_0^a \int_0^b \Psi_m(x, y) e^{-i(\alpha x + \gamma y)} \, dy \, dx \times \int_0^a \int_0^b \Psi_n(x, y) e^{i(\alpha x + \gamma y)} \, dy \, dx \quad (12g)$$

The integrals in Eqs. (12c), (12d), and (12g) can be performed analytically for most panel eigenfunctions. Equations (12e) and (12f), which define the aerodynamic influence functions, must be evaluated numerically.

Piston Theory Generalized Forces

Piston theory is presented here for comparison with the full potential flow solution developed previously. Piston theory assumes that the pressure acting on the panel is equivalent to the pressure acting on a piston in a tube:

$$p = \rho_a a_\infty \left(\frac{\partial w}{\partial t} + U_a \frac{\partial w}{\partial x} \right) \tag{13}$$

The total piston velocity includes a convection term $U_a(\partial w/\partial x)$, as well as a direct velocity term $\partial w/\partial t$. Here the plate is the equivalent piston and the tube is perpendicular to the plate.

Combining Eqs. (2) and (13) and inserting into Eq. (6) yields the piston theory generalized aerodynamic forces

$$Q_n(t) = \sum_{m=1}^{N} Q_{mn}(t) \tag{14a}$$

where

$$Q_{mn}(t) = q_m(t) S_{mn} + \dot{q}_m(t) D_{mn} \tag{14b}$$

$$S_{mn} = \frac{1}{M} \int_0^a \int_0^b \frac{\partial \Psi_m}{\partial x} \Psi_n \, dy \, dx \tag{14c}$$

$$D_{mn} = \frac{1}{MU_a} \int_0^a \int_0^b \Psi_m \Psi_n \, dy \, dx \tag{14d}$$

Note that this result is identical to that obtained from full potential flow analysis if the influence functions $[H_{mn}(t)$ and $I_{mn}(t)]$ are ignored.

Approximate Generalized Forces

Many techniques for approximating the aerodynamic loads on structures (mainly wing sections) have been published in the past. Jones[11] was one of the earliest, whereas Leishman[12] and Morino et al.[3] have more recently investigated Laplace/frequency domain approximations of the aerodynamic loads. However, the form of the aerodynamic forces expressed in Eqs. (12) does not lend itself to direct application of these methods. Utilization of the techniques in Refs. 1, 9, and 10 would require transforming the time domain representations in Eqs. (12) to the frequency domain. This additional computational step would introduce more error into the solution. Therefore, a more direct time domain approximation technique was sought.

Since the generalized aerodynamic forces represented in Eq. (12b) are functions of the panel generalized coordinates, they can be viewed as dynamic feedback on the panel. These feedback dynamics are characterized by the influence functions $H_{mn}(t)$ and $I_{mn}(t)$, which represent aerodynamic impulse responses, and the influence coefficients S_{mn} and D_{mn}, which are instantaneous or feedthrough dynamics.

Since there is no closed-form solution for the generalized forces, some approximation must be made. The approach suggested here is to construct digital filters that approximate these dynamics. A finite impulse response (FIR) filter of the form:

$$P(z) = \sum_{i=0}^{R-1} h(iT) z^{-i} \tag{15}$$

exactly represents a dynamic system having a discrete time impulse response $h(iT)$ and a z-domain transfer function $P(z)$ (Ref. 13). In this case the dynamic system is the aerodynamics represented by Eq. (12b), which has two impulse responses of $H_{mn}(iT)$ and $I_{mn}(iT)$. Note that $H_{mn}(iT)$ and $I_{mn}(iT)$ are discrete time approximations of Eqs. (12e) and (12f).

Equation (15) can be used to represent the aerodynamics of Eq. (12b) by substituting a numerically calculated influence function $[H_{mn}(iT)$ or $I_{mn}(iT)]$ for $h(iT)$ in Eq. (15). However, constructing a state-space model of an FIR filter requires as many states as filter coefficients. Therefore, any reasonable discrete temporal resolution of the influence functions would result in a very high-order state-space model.

Fortunately, a reduced order recursive filter may be constructed by applying Prony's method to the influence functions.[14,15] Prony's method approximates an impulse response (in this case the influence functions) with a set of exponential functions in a least-squares sense. These exponential approximations to the influence functions can be readily transformed into an Ith order IIR filter of the form:

$$\hat{P}_{mn}(z) = \sum_{i=0}^{I-1} a_i z^{-i} \Big/ \sum_{i=0}^{I-1} b_i z^{-i} \tag{16}$$

Equating like powers of the FIR representation in Eq. (15) with the IIR representation of Eq. (16), and replacing the temporal argument iT with subscripts, yields an overdetermined set of equations (for $R >> I$) of the form:

$$\begin{Bmatrix} a \\ 0 \end{Bmatrix} = \begin{bmatrix} h_1 \\ h_2 \end{bmatrix} \{b\} \tag{17a}$$

where

$$\begin{Bmatrix} a \\ 0 \end{Bmatrix} = \begin{Bmatrix} a_0 \\ a_1 \\ \vdots \\ a_{I-1} \\ 0 \\ 0 \\ \vdots \\ 0 \end{Bmatrix} \tag{17b}$$

$$\begin{bmatrix} h_1 \\ h_2 \end{bmatrix} = \left[\begin{array}{cccc} h_0 & 0 & \cdots & 0 \\ h_1 & h_0 & \cdots & 0 \\ \vdots & \vdots & & \vdots \\ h_{I-1} & h_{I-2} & \cdots & 0 \\ \hline h_I & h_{I-1} & \cdots & h_0 \\ h_{I+1} & h_I & \cdots & h_1 \\ \vdots & & \vdots & \vdots \\ h_{R-1} & h_{R-2} & \cdots & h_{R-I-1} \end{array}\right] \tag{17c}$$

$$\{b\} = \begin{Bmatrix} b_0 \\ b_1 \\ \vdots \\ b_{I-1} \end{Bmatrix} \tag{17d}$$

The lower portion of this system of equations, $0 = h_2 b$ is solved, in a least-square sense, to give the denominator coefficients b_i in Eq. (16). Then the numerator coefficients a_i can be found uniquely from the upper portion of Eq. (17a), $a = h_1 b$.

At this point, the approximate filter of Eq. (16) can be converted to a continuous time (Laplace domain) representation through a bilinear transformation. This transformation is accomplished by substituting for z in Eq. (16) as follows:

$$z = \frac{1 + (T/2)\kappa}{1 - (T/2)\kappa} \tag{18}$$

Note that care should be taken in the selection of T. Significant errors can result if the sample period is not sufficiently small. Application of the bilinear transformation results in a continuous time filter of the form:

$$\hat{P}_{mn}(\kappa) = \sum_{i=0}^{I-1} \hat{a}_i \kappa^i \Big/ \sum_{i=0}^{I-1} \hat{b}_i \kappa^i \tag{19}$$

where $\hat{a}_i$ and $\hat{b}_i$ are new coefficients.

As an example, suppose the values of the influence function $H_{mn}(iT)$ are used to solve for the filter coefficients in Eq. (17a). When provided with an input signal that represents the panel generalized coordinate $q_m(iT)$, this filter would output an approximate convolution of $q_m(iT)$ with $H_{mn}(iT)$. Similarly, a filter could be constructed from $I_{mn}(iT)$ and provided with a signal representing $\dot{q}_m(iT)$. Summing the outputs of the two filters would yield an approximation to the dynamic portion of Eq. (12b). This process will be covered in more detail later.

The accuracy of this type of approximation is demonstrated in Fig. 2. This plot shows the generalized force Q_{11} for a unit step change in the generalized coordinate q_1, as represented in Eq. (12b). The results are presented for a panel of aspect ratio $a/b = 1.0$, mass ratio $\mu = 0.1$, and $M = 2.0$. Three curves are shown, one representing direct calculation from the influence function $H_{11}(iT)$, while the others represent the step response of an 8th- and 16th-order approximating filter with a sample period of $T = 0.1$. As one would expect, the higher-order filter yields higher accuracy. Other influence functions exhibit similar accuracy.

An approximate filter can be found, as shown previously, for each $H_{mn}(t)$ and $I_{mn}(t)$. A complete set of these filters can then be summed according to Eqs. (12a) and (12b). This would yield a dynamic system that has the generalized coordinates $q_m(t)$ and $\dot{q}_m(t)$ as the inputs, and the generalized aerodynamic forces $Q_n(t)$ as the outputs. This system is then coupled as

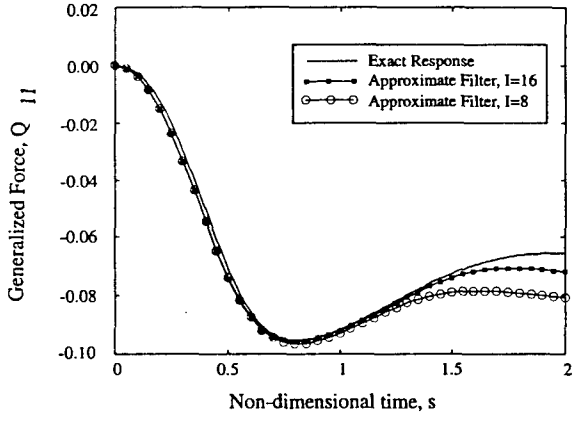

Fig. 2 Generalized force step response for exact and two approximating filters.

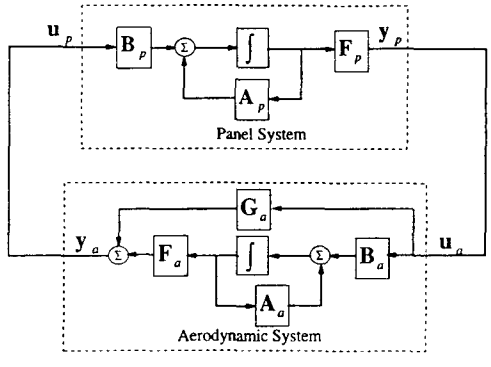

Fig. 3 State-space schematic of the complete aeroelastic system.

feedback on the panel resulting in a complete aeroelastic system. This is shown schematically (in state-space notation) in Fig. 3 and will be discussed in more detail in the next section.

State-Space Formulation

The general equation of motion for the panel, described in Eq. (3), in the absence of structural damping, can be expressed in state-space form as

$$\dot{\boldsymbol{x}}_p = A_p \boldsymbol{x}_p + B_p \boldsymbol{u}_p \tag{20a}$$

$$\boldsymbol{y}_p = F_p \boldsymbol{x}_p \tag{20b}$$

where

$$\boldsymbol{x}_p = \{q_1 \quad q_2 \quad \cdots \quad q_n \quad \dot{q}_1 \quad \dot{q}_2 \quad \cdots \quad \dot{q}_n\}^T \tag{20c}$$

$$A_p = \begin{bmatrix} 0 & 0 & \cdots & 0 & 1 & \cdots & 0 \\ \vdots & \vdots & \ddots & \vdots & \vdots & \ddots & \vdots \\ 0 & 0 & \cdots & 0 & 0 & \cdots & 1 \\ -\omega_1^2 & 0 & \cdots & 0 & 0 & \cdots & 0 \\ 0 & -\omega_2^2 & \cdots & 0 & 0 & \cdots & 0 \\ \vdots & \vdots & \ddots & \vdots & \vdots & \ddots & \vdots \\ 0 & 0 & \cdots & -\omega_n^2 & 0 & \cdots & 0 \end{bmatrix} \tag{20d}$$

$$B_p = \rho_a U_a^2 \begin{bmatrix} 0 & 0 & \cdots & 0 \\ 0 & 0 & \cdots & 0 \\ \vdots & & \ddots & \vdots \\ 0 & 0 & \cdots & 0 \\ \dfrac{-1}{M_1} & 0 & \cdots & 0 \\ 0 & \dfrac{-1}{M_2} & \cdots & 0 \\ \vdots & & \ddots & \vdots \\ 0 & 0 & \cdots & \dfrac{-1}{M_n} \end{bmatrix} \tag{20e}$$

$$\boldsymbol{u}_p = \{Q_1(t) \quad Q_2(t) \quad \cdots \quad Q_n(t)\}^T \tag{20f}$$

$$F_p = \begin{bmatrix} 1 & 0 & \cdots & 0 & 0 & 0 & \cdots & 0 \\ 0 & 0 & \cdots & 0 & 1 & 0 & \cdots & 0 \\ 0 & 1 & \cdots & 0 & 0 & 0 & \cdots & 0 \\ 0 & 0 & \cdots & 0 & 0 & 1 & \cdots & 0 \\ \vdots & \vdots & & \vdots & \vdots & \vdots & & \vdots \\ 0 & 0 & \cdots & 1 & 0 & 0 & \cdots & 0 \\ 0 & 0 & \cdots & 0 & 0 & 0 & \cdots & 1 \end{bmatrix} \tag{20g}$$

such that the output vector, which is equivalent to the input of the aerodynamic system, is a reordered version of the panel state vector:

$$\boldsymbol{y}_p = \{q_1 \quad \dot{q}_1 \quad q_2 \quad \dot{q}_2 \quad \cdots \quad q_n \quad \dot{q}_n\}^T \tag{20h}$$

A filter of the form in Eq. (19) can be cast in state variable form as follows:

$$\boldsymbol{x}_{\hat{p}} = A_{\hat{p}} \boldsymbol{x}_{\hat{p}} + B_{\hat{p}} \boldsymbol{u}_{\hat{p}} \tag{21a}$$

$$\boldsymbol{y}_{\hat{p}} = F_{\hat{p}} \boldsymbol{x}_{\hat{p}} + G_{\hat{p}} \boldsymbol{u}_{\hat{p}} \tag{21b}$$

where

$$A_{\hat{p}} = \begin{bmatrix} -\hat{b}_2/\hat{b}_1 & -\hat{b}_3/\hat{b}_1 & \cdots & -\hat{b}_{I-1}/\hat{b}_1 & -\hat{b}_I/\hat{b}_1 \\ 1 & 0 & \cdots & 0 & 0 \\ 0 & 1 & \cdots & 0 & 0 \\ \vdots & \vdots & \ddots & \vdots & \vdots \\ 0 & 0 & \cdots & 1 & 0 \end{bmatrix} \tag{21c}$$

$$B_{\hat{p}} = \begin{bmatrix} 1 \\ 0 \\ \vdots \\ 0 \end{bmatrix} \tag{21d}$$

$$F_{\hat{p}} = [\hat{a}_2/\hat{b}_1 - \hat{a}_1\hat{b}_2/\hat{b}_1^2 \quad \hat{a}_3/\hat{b}_1 - \hat{a}_1\hat{b}_3/\hat{b}_1^2 \quad \cdots \quad \hat{a}_r/\hat{b}_1 - \hat{a}_1\hat{b}_r/\hat{b}_1^2] \tag{21e}$$

$$G_{\hat{p}} = [\hat{a}_1/\hat{b}_1] \tag{21f}$$

The input is the appropriate panel generalized coordinate and the output is the approximate convolution of the generalized coordinate and the influence function used in the filter calculation of Eq. (17a). The states of the previous system are of mathematical construct and have no physical significance.

At this point a representation of Eq. (12b) can be constructed for a single plate mode ($m = n$) as follows:

1) The appropriate influence functions $H_{mm}(iT)$ and $I_{mm}(iT)$ are found by the numeric integration of Eqs. (12e) and (12f).

2) Two filters are constructed by solving Eq. (17a) for the filter coefficients, one based on $H_{mm}(iT)$ and the other based on $I_{mm}(iT)$.

3) Each of these two filters is transformed to continuous time using Eq. (18) and cast in state variable form according to Eq. (21a). In general, the state variable representations associated with $H_{mn}(iT)$ and $I_{mn}(iT)$ will be referred to as the sets $\{A_{H_{mn}}, B_{H_{mn}}, F_{H_{mn}}, G_{H_{mn}}\}$ and $\{A_{I_{mn}}, B_{I_{mn}}, F_{I_{mn}}, G_{I_{mn}}\}$, respectively.

4) Finally, the state variable representations are combined according to Eq. (12b) as follows:

$$\dot{x}_a = A_a x_a + B_a u_a \tag{22a}$$

$$y_a = F_a x_a + G_a u_a \tag{22b}$$

where

$$y_a = Q_{mn}(t) \tag{22c}$$

$$u_a = \{q_m \quad \dot{q}_m\}^T \tag{22d}$$

$$A_a = \begin{bmatrix} A_{H_{mm}} & 0 \\ 0 & A_{I_{mm}} \end{bmatrix} \tag{22e}$$

$$B_a = \begin{bmatrix} B_{H_{mm}} & 0 \\ 0 & B_{I_{mm}} \end{bmatrix} \tag{22f}$$

$$F_a = [F_{H_{mm}} \quad F_{I_{mm}}] \tag{22g}$$

and the influence coefficients of Eqs. (12c) and (12d) are incorporated as follows:

$$G_a = [G_{H_{mm}} + S_{mm} \quad G_{I_{mm}} + D_{mm}] \tag{22h}$$

The previous representation would be sufficient if the panel model had only one mode. This would result in only one term in the sum given by Eq. (12a). Multiple panel modes require the extension of the previous representation to include all appropriate influence functions. This more general representation is as follows:

$$\dot{x}_a = A_a x_a + B_a u_a \tag{23a}$$

$$y_a = F_a x_a + G_a u_a \tag{23b}$$

where

$$y_a = \{Q_1(t) \quad Q_2(t) \quad \cdots \quad Q_n(t)\}^T \tag{23c}$$

$$u_a = \{q_1 \quad \dot{q}_1 \quad q_2 \quad \dot{q}_2 \quad \cdots \quad q_n \quad \dot{q}_n\}^T \tag{23d}$$

$$A_a = \begin{bmatrix} A_{H_{11}} & 0 & \cdots & 0 & 0 \\ 0 & A_{I_{11}} & \cdots & 0 & 0 \\ \vdots & \vdots & \ddots & \vdots & \vdots \\ 0 & 0 & \cdots & A_{H_{mn}} & 0 \\ 0 & 0 & \cdots & 0 & A_{I_{mn}} \end{bmatrix} \tag{23e}$$

$$B_a = \begin{bmatrix} B_{H_{11}} & 0 & \cdots & 0 & 0 \\ 0 & B_{I_{11}} & \cdots & 0 & 0 \\ \vdots & \vdots & \ddots & \vdots & \vdots \\ 0 & 0 & \cdots & B_{H_{1n}} & 0 \\ 0 & 0 & \cdots & 0 & B_{I_{1n}} \\ \vdots & \vdots & \vdots & \vdots & \vdots \\ B_{H_{m1}} & 0 & \cdots & 0 & 0 \\ 0 & B_{I_{m1}} & \cdots & 0 & 0 \\ \vdots & \vdots & \ddots & \vdots & \vdots \\ 0 & 0 & \cdots & B_{H_{mn}} & 0 \\ 0 & 0 & \cdots & 0 & B_{I_{mn}} \end{bmatrix} \tag{23f}$$

$$F_a = \begin{bmatrix} F_{H_{11}} & F_{I_{11}} & \cdots & F_{H_{1n}} & F_{I_{1n}} \\ F_{H_{21}} & F_{I_{21}} & \cdots & F_{H_{2n}} & F_{I_{2n}} \\ \vdots & \vdots & \ddots & \vdots & \vdots \\ F_{H_{m1}} & F_{I_{m1}} & \cdots & F_{H_{mn}} & F_{I_{mn}} \end{bmatrix} \tag{23g}$$

$$G_a = \begin{bmatrix} G'_{H_{11}} & G'_{I_{11}} & \cdots & G'_{H_{1n}} & G'_{I_{1n}} \\ G'_{H_{21}} & G'_{I_{21}} & \cdots & G'_{H_{2n}} & G'_{I_{2n}} \\ \vdots & \vdots & \ddots & \vdots & \vdots \\ G'_{H_{m1}} & G'_{I_{m1}} & \cdots & G'_{H_{mn}} & G'_{I_{mn}} \end{bmatrix} \tag{23h}$$

and the influence coefficients are incorporated as follows:

$$G'_{H_{mn}} = G_{H_{mn}} + S_{mn} \tag{23i}$$

$$G'_{I_{mn}} = G_{H_{mn}} + D_{mn} \tag{23j}$$

The panel and aerodynamic state-space models can then be coupled together as shown in Fig. 3.

The size of the state-space model can be further reduced by taking advantage of certain symmetries in the influence functions. The greatest reduction can be had by noting that $H_{mn} = -H_{nm}$ and $I_{mn} = -I_{nm}$. Furthermore, if more than one expansion mode is used in the spanwise direction for a simply supported plate, the influence functions can be indexed such that $H_{mn} \rightarrow H_{pqrs}$ and $I_{mn} \rightarrow I_{pqrs}$. In this case, those influence functions where $|q - s|$ is odd, are zero.

Results

To validate the coupled model, the system parameters were varied and the flutter boundaries were compared to results from the literature. Flutter boundaries were found by increasing the nondimensional dynamic pressure λ and calculating the coupled system eigenvalues. Flutter instability occurs when at least one of the system eigenvalues lies in the right half-plane.

This is demonstrated in Fig. 4, which shows the distribution of the system eigenvalues. Note the distribution of the approximate aerodynamic eigenvalues. Those eigenvalues associated with the panel modes are contained in the zoom region indicated in Fig. 4. These results are for a panel with $a/b = 1.0$, $\mu = 0.1$, $M = 2.0$, and using a four-mode expansion [i.e., $N = 4$ in Eq. (2)]. In this case, the frequency is nondimensionalized such that $k = (\omega a/U_a)(\lambda/\mu)^{1/2}$.

Figure 5 is an expanded view of the zoom region of Fig. 4 and depicts the pole migration with increasing dynamic pressure. In Fig. 5 eigenvalues at different dynamic pressure are connected with a line. Note the path of the complex conjugate eigenvalue pair as they enter the right half-plane. Also note that the only eigenvalues that experience significant migration are the complex conjugate pairs that are associated with the panel modes. One of these two migrating pairs is the eigenvalue that becomes unstable.

Another important piece of information that can be obtained from the eigenvalue locus in Fig. 5 is the frequency of flutter. In Fig. 5 the frequency of flutter is between the first and second natural frequencies of the panel. This is consistent with the

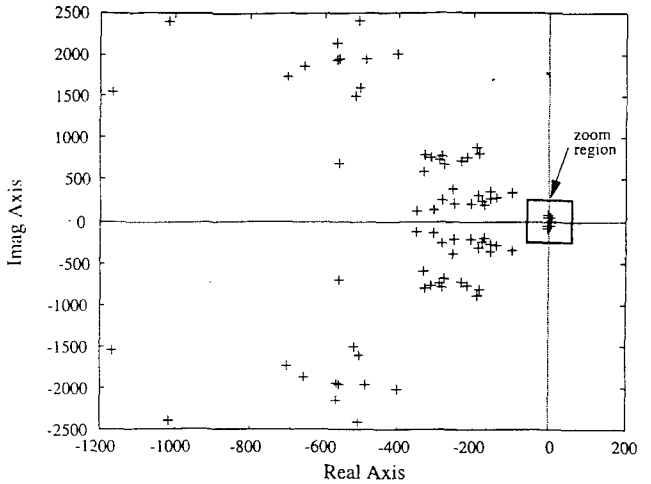

Fig. 4 Locus of system eigenvalues with varying dynamic pressure.

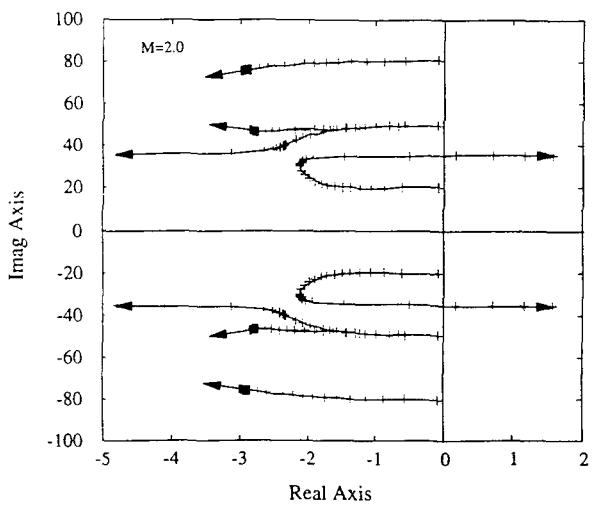

Fig. 5 Close-up locus of system eigenvalues with varying dynamic pressure, $M = 2.0$.

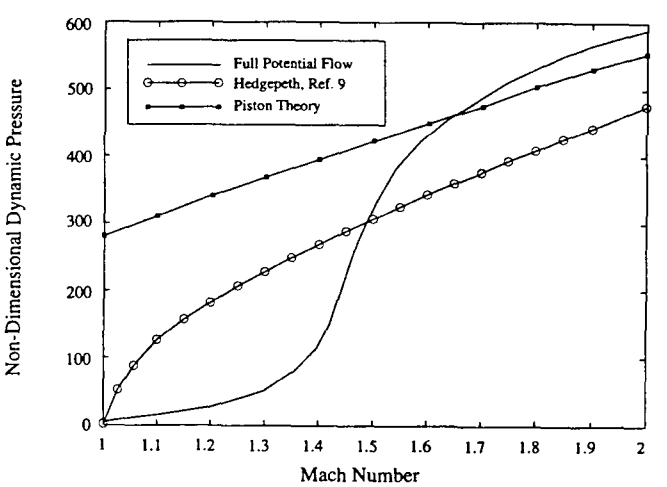

Fig. 6 Flutter dynamic pressure vs Mach number for $a/b = 0$.

A comparison of flutter dynamic pressure vs Mach number is shown in Fig. 6. Results are illustrated for a panel with $\mu = 0.1$ and $a/b = 0$ (i.e., an infinitely wide panel). Also included in the figure are the flutter boundaries for a piston theory model and for an approximate, quasisteady aerodynamic flutter boundary described by Hedgepeth.[9]

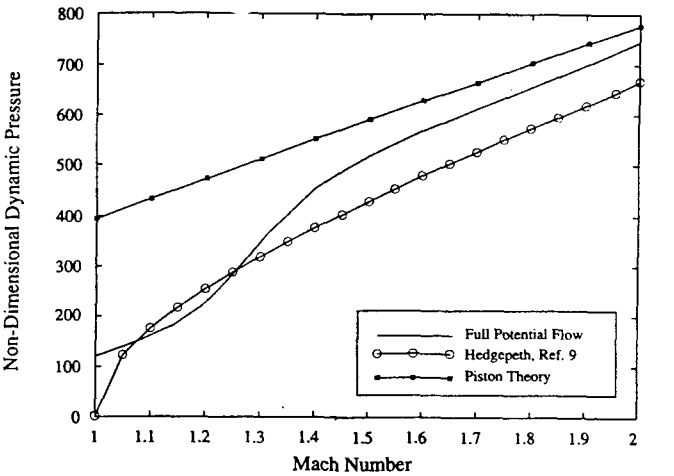

Fig. 7 Flutter dynamic pressure vs Mach number for $a/b = 1$.

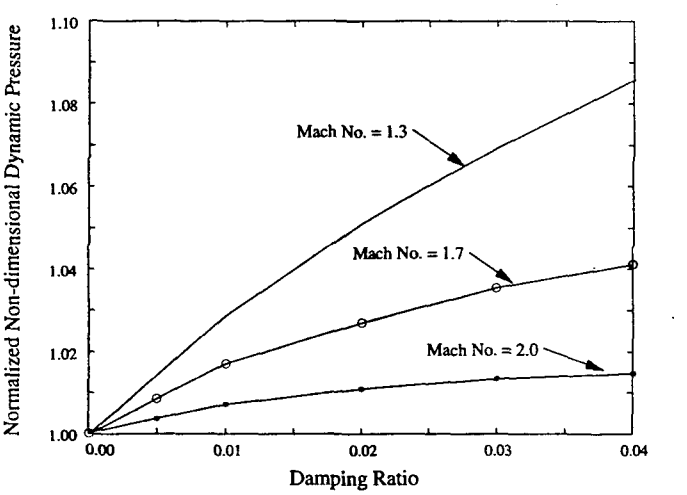

Fig. 8 Flutter dynamic pressure vs damping ratio.

Note in Fig. 6 that the three theories approach each other asymptotically as the Mach number increases. However, for Mach numbers below 1.5, the theory incorporating linearized potential flow aerodynamics predicts flutter boundaries well below the others. Full potential flow theory predicts a minimum flutter dynamic pressure of zero at a Mach number of 1.0. These results are consistent with those obtained by Dowell.[6,7]

A similar flutter boundary, for a square panel (i.e., $a/b = 1.0$) with $\mu = 0.1$ and using a four-mode expansion, is shown in Fig. 7. These results are also consistent with those obtained by Dowell. Note in this case the minimum flutter dynamic pressure is nonzero.

A final and interesting result is the effect of proportional modal damping on the flutter dynamic pressure. Figure 8 shows the flutter dynamic pressure, normalized with respect to the undamped flutter dynamic pressure, as a function of the modal damping ratio for three different Mach numbers. Proportional damping is modeled as an additional term of the form $2\zeta\omega_n\dot{q}_n$ to Eq. (3). Note that proportional damping has the greatest effect on flutter dynamic pressure at lower Mach numbers.

Conclusions

A new method for modeling the aerodynamic loading of panels that incorporates linearized potential flow aerodynamics has been developed. This was accomplished by approximating the aerodynamic generalized forces on the panel with discrete time filters. These filters were coupled as feedback to the in vacuo panel model. The accuracy of the method was demon-

strated by comparing results of this model with results obtained in previous work. Future work will use this new aeroelastic model in optimal control studies.

Acknowledgments

This work was supported in part by the Air Force Office of Scientific Research, Contract Monitor Jim Chang C.I.P.I., and the National Science Foundation Graduate Traineeship EE-92-56573.

References

[1]Dugundji, J., "Theoretical Considerations of Panel Flutter at High Supersonic Mach Numbers," *AIAA Journal*, Vol. 4, No. 7, 1966, pp. 1257–1266.

[2]Gray, C. E., and Mei, C., "Large Amplitude Finite Element Analysis of Composite Panels in Hypersonic Flow," *Proceedings of the AIAA Dynamics Specialist Conference*, AIAA, Washington, DC, 1992, pp. 127–132.

[3]Morino, L., Mastroddi, F., De Troia, R., Ghiringhelli, G. L., and Mantegazza, P., "Matrix Fraction Approach for Finite-State Aerodynamic Modeling," *AIAA Journal*, Vol. 33, No. 4, 1995, pp. 703–711.

[4]Leishman, J. G., and Nguyen, K. Q., "State-Space Representation of Unsteady Airfoil Behavior," *AIAA Journal*, Vol. 28, No. 5, 1989, pp. 836–844.

[5]Dowell, E. H., "Generalized Aerodynamic Forces on a Flexible Plate Undergoing Transient Motion," *Quarterly of Applied Mathematics*, Vol. 26, No. 3, 1967, pp. 2267–2270.

[6]Dowell, E. H., *Aeroelasticity of Plates and Shells*, Noordhoff International, Leyden, The Netherlands, 1975.

[7]Dowell, E. H., "Panel Flutter: A Review of the Aeroelastic Stability of Plates and Shells," *AIAA Journal*, Vol. 8, No. 3, 1970, pp. 385–399.

[8]Johns, D. J., "A Panel Flutter Review," *Manual on Aeroelasticity, Part III*, AGARD, 1969, Chap. 7.

[9]Hedgepeth, J. M., "Flutter of Rectangular Simply Supported Panels at High Supersonic Speeds," *Journal of the Aeronautical Sciences*, Vol. 24, No. 8, 1957, pp. 563–573.

[10]Meirovitch, L., *Analytical Methods in Vibrations*, Macmillan, New York, 1967.

[11]Jones, R. T., "The Unsteady Lift of a Wing of Finite Aspect Ratio," NACA Rept. 681, 1940.

[12]Leishman, J. G., "Validation of Approximate Indicial Aerodynamic Functions for Two-Dimensional Subsonic Flow," *Journal of Aircraft*, Vol. 25, No. 10, 1988, pp. 914–922.

[13]Haykin, S., *Adaptive Filter Theory*, 2nd ed., Prentice–Hall, Englewood Cliffs, NJ, 1991.

[14]Evans, A. G., and Fischl, R., "Optimal Least Squares Time-Domain Synthesis of Recursive Digital Filters," *IEEE Transactions on Audio and Electroacoustics*, Vol. AU-21, No. 1, 1973, pp. 61–65.

[15]Marple, S. L., *Digital Spectral Analysis with Applications*, Prentice–Hall, Englewood Cliffs, NJ, 1987.